Static simulations of CaF_2 polymorphs

A. Martín Pendás, J. M. Recio, M. Flórez, and Víctor Luaña
Departamento de Química Física y Analítica, Facultad de Química, Universidad de Oviedo, 33006 Oviedo, Spain

M. Bermejo
Departamento de Física, Facultad de Ciencias, Universidad de Oviedo, 33006 Oviedo, Spain
(Received 8 November 1993)

Combined first-principles pairwise simulations and quantum-mechanical *ab initio* perturbed ion (AIPI) calculations have been extensively performed to determine the static equations of state (EOS) of the cubic (fluorite-type) and orthorhombic (α-$PbCl_2$-type) polymorphs of CaF_2. This theoretical investigation covers the range of pressures experimentally available (0–45 GPa). The elastic behavior and the equilibrium crystal parameters have been accurately determined by means of efficient numerical procedures involving a Richardson-iterated, finite-difference formula for the derivatives and the combination of downhill simplex and modified Powell methods for the multidimensional optimizations. For the bulk modulus and the effective elastic constants of the cubic phase, the simulations and AIPI calculations give increasing functions of pressure with small negative curvatures. Besides, the zero-pressure AIPI computations agree with the values of Catlow *et al.* [J. Phys. C **11**, 3197 (1978)] for the bulk modulus and the elastic constants. The computed EOS also reproduces quantitatively the most recent experimental p-V data for the cubic phase. For the orthorhombic phase, we optimize nine crystal parameters for each value of pressure. This set provides a full structural characterization of this phase, as well as a global description of the p-V relationship that is consistent with the synchrotron-radiation x-ray-diffraction study of Gerward *et al.* [J. Appl. Cryst. **25**, 578 (1992)]. Our simulation techniques are able to detect a first-order phase transition from the low-pressure fluorite-type to the high-pressure α-$PbCl_2$-type polymorph. The computed thermodynamic transition pressure lies below the experimental values, as it should for this kind of structural transformation exhibiting large pressure hysteresis.

I. INTRODUCTION

In 1980, Oberschmidt and Lazarus[1] investigated, in a series of three experimental papers, the dependence of the ionic conductivity (σ) on temperature (T) and pressure (p) for several lead and alkaline earth dihalides with a common formula of AX_2. For some of these compounds, they observed pressure-induced phase transitions from cubic-to-orthorhombic structures (with large pressure hysteresis at low temperatures), where the cubic polymorph is the phase with higher ionic conductivity. These authors found that σ increases with T and proposed different ionic mechanisms to explain the conductivity associated with the regions of different slopes in the σ-T curves.

The number of experimental investigations on compounds able to conduct electricity through ionic mobility increased considerably in the past decade[2,3] and provided physical explanations to the unusually high-ionic conductivity exhibited at high temperatures by CaF_2 and other crystals with fluorite structure. This behavior is now understood as the result of a quasi-melting of the anionic sublattice at temperatures well below the melting point of the crystal. Such a response leads to a structurally highly disordered state which is called the superionic phase of the crystal.

For studying such disordered systems as superionic conductors, Shimojo and Okazaki[4] have remarked the convenience of using computer simulation methods and, in particular, molecular dynamics. Indeed, molecular dynamics calculations, fed commonly with rigid pairwise empirical potentials, have been extensively performed during the last decade on fluorite-type superionic materials by Parrinello *et al.*[5] and by Gillan and co-workers (see cites quoted in Refs. 4 and 6). Very recently, Lindan and Gillan[6] have studied superionic conduction in CaF_2 by means of a new code that combines the molecular dynamics technique with the shell-model treatment of the electronic polarization in the interionic potentials. They concluded that the explicit inclusion of electronic polarizability causes remarkably small modifications on both static and dynamic quantities.

Besides the technological importance of such fluorite-type crystals as superionic conductors, CaF_2 has been proposed in the earlier 80s as an internal pressure standard in single-crystal diffraction experiments covering simultaneously high-temperature and high-pressure conditions. Hazen and Finger[7] have justified this choice in terms of eight requirements that an ideal p and T x-ray standard should satisfy. Following that paper, an important amount of experimental work has enlarged our knowledge on the behavior of CaF_2 under different p and T conditions.

The most recent high-pressure, high-temperature equation of state (EOS) for cubic CaF_2 has been reported by Angel,[8] who combined room temperature single-

crystal x-ray-diffraction measurements up to 9 GPa with available thermodynamic data. Angel has remarked on the necessity of a reevaluation of this EOS due to "disagreements in the literature regarding the value of the bulk modulus of fluorite."

An extensive investigation of the CaF_2 response to pressure has been carried out by Gerward *et al.*[9] They performed synchrotron-radiation x-ray-diffraction studies covering the range 0–45 GPa and observed a phase transition from the cubic (fluorite-type, $C1$ from now on) to the orthorhombic (α-$PbCl_2$-type, $C23$ from now on) structure at about 9.5 GPa. The transition was found to be at least partially quenchable and, according to Angel *et al.*,[10] the kinetics could therefore play a decisive role since this kind of transition "includes thermally activated processes such as atomic ordering within a crystal structure." The metastable high-pressure phase has also been studied at zero pressure by Gerward *et al.*[9] However, due to the damage suffered by the single crystal in the phase transition, only partial characterization of the crystal parameters is reported for the $C23$ polymorph.

The investigation described in this paper is intended to constitute a practical tool in the two main fields mentioned above (superionicity and pressure calibration) that make CaF_2 a current technologically interesting material. To accomplish that challenge, we have combined, for total energy calculations, quantum-mechanical[11–13] and first-principles pairwise[14] strategies. In addition, we have used efficient numerical procedures able to locate minimum energy configurations in n-dimensional surfaces and to compute the derivatives of multivariable functions with high precision (see Refs. 15 and 16).

Regarding superionicity, our contribution is limited to the computational aspects, since we are restricted in this work to static simulations. We provide, however, a set of reliable interionic potentials derived from quantum-mechanical descriptions of ions in a wide range of pressure and temperature crystalline situations. These theoretical potentials may be introduced with confidence in computer assisted simulations far away from the ambient conditions often used to derive the empirical potentials currently employed.[6] Virtues of the results obtained using our set of interionic potentials are (a) the overall agreement with experimental data in a variety of cohesive and elastic properties, (b) the successful description of the room temperature EOS observed for CaF_2 in both the cubic and orthorhombic phases, and (c) the good prediction of thermodynamic data involved in the pressure-induced phase transition.

Regarding pressure calibration, we have been able to quantitatively reproduce the behavior of CaF_2 polymorphs over the whole range of available data. Our computed volume-pressure and elastic-constant–pressure curves for the cubic fluorite structure agree with the most recent x-ray-diffraction experiments[8,9] and extend the information on the elastic behavior of this polymorph to a larger pressure range. For the orthorhombic structure, where the experimental data are scarce and the uncertainties are larger due to the difficulties of single-crystal studies, our computed predictions represent a full characterization of the unit cell parameters and the internal coordinates.

The organization of the rest of the paper is the following. In Sec. II, we describe the variety of simulation techniques that we have used to compute total energies, crystal parameters, and elastic constants. Section III deals simultaneously with the results and the discussion, and it is divided into three subsections. The low- and high-pressure EOS are described separately in the two first subsections. The stability and the phase transition data are analyzed in the last one. The conclusions and comments on prospective work end the paper.

II. SIMULATION TECHNIQUES

A. Total energy

The actual crystalline phase exhibited by CaF_2 depends experimentally on the history of the sample, as well as on the pressure and temperature conditions. The unit cell descriptions of the $C1$ and $C23$ structures of this compound are collected in Table I. $C1$ belongs to the $Fm3m$ space group with the cubic cell length (a) its single free geometrical parameter. $C23$ belongs to the orthorhombic $Pbnm$ space group and is characterized by specifying nine values: the three unit cell lengths (a, b, c) and the x and y coordinates of its three nonequivalent ions, one calcium (Ca) and two fluorines (F1,F2).

In the investigation on these polymorphs, we have followed two different theoretical approaches to compute their total energy at each given set of geometrical parameters. The first is a pair interaction model implemented using a computational code called PAIRPOT. The second is the *ab initio* perturbed-ion model (AIPI),[12] a quantum-mechanical technique that has been successfully applied

TABLE I. Structural data for the unit cells of the $C1$ and $C23$ phases of CaF_2.

Crystallographic system	Cubic, $C1$	Orthorhombic, $C23$
Space group	$Fm3m$	$Pbnm$
Cell parameters	$a = b = c$	$a \neq b \neq c$
	$\alpha = \beta = \gamma = 90$	$\alpha = \beta = \gamma = 90$
Atomic positions	Ca (4a) (0,0,0)	Ca (4c) [x(Ca),y(Ca),$\frac{1}{4}$]
	F (8c) ($\frac{1}{4}$, $\frac{1}{4}$, $\frac{1}{4}$)	F1 (4c) [x(F1),y(F1),$\frac{1}{4}$]
		F2 (4c) [x(F2),y(F2),$\frac{1}{4}$]

to the description of pure and defective closed-shell crystals in the past five years.[11,13,15] Pair potentials derived from AIPI calculations have been used in the PAIRPOT runs, aimed to help AIPI in exploring the multidimensional energy hypersurface.

The PAIRPOT code is intended as a general and flexible tool in the computation of static thermodynamic properties of pure crystals from rigid (nonpolarizable) pair potentials. Its main feature lies in the simplicity and degree of automation. The program computes the 0 K molar Gibbs energy of a given lattice. This function involves three fundamental terms: (a) the classical Madelung long-range contribution, obtained by means of the Ewald transformation; (b) the nonclassical short-range pairwise model energy, obtained by adding interactions until an user-supplied energy convergence threshold is achieved; and (c) the pressure-volume term. The distance range used for the computation of short-range pairwise contributions may be determined by indicating the number of neighbors (set of equivalent ions located at the same radial distance from a chosen one) surrounding every nonequivalent ion that is to be used up in the pair summation. This possibility allows us to easily construct first, second, or nth neighbors models to be compared with the ordinary nearest-neighbor pairwise simulations found in the literature.

The PAIRPOT code has been fed in this work with nonempirical Ca^{2+}-F^- and F^--F^- short-range pairwise potentials (see Table II) derived from the method described in Ref. 14. The most remarkable peculiarities of this procedure are (a) the energetic interactions are computed from the AIPI descriptions of the ions for a wide range of lattice parameters; and (b) the interatomic potentials include pairwise modeled contributions from the many-body deformation of the ions upon crystal formation. The potentials so obtained may be safely used in theoretical simulations where the values of the lattice parameters are far away from those found at the energy minimum. In particular, they are well suited then for high-temperature or high-pressure calculations. The short-range parts of the Ca^{2+}-F^- and F^--F^- potentials used in this work have minimum and maximum cutoff radii of 3 and 20 bohrs. The Ca^{2+}-Ca^{2+} potential contains only the point charge contribution because nonclassical interactions are negligible. The total energy or Gibbs potential has been obtained within 10^{-6} hartree.

For a detailed description of the AIPI method we refer to previous papers.[11,12,15,17] It is interesting to bear in mind that the method solves the Hartree-Fock (HF) equations of the solid in a localized Fock space by breaking the crystal wave function into local, nearly orthogonal group functions (atomic or ionic in nature). The localized nature of this procedure has, for our purposes, a number of advantages over the canonical approach,[18] namely: (a) A localized picture is much better suited to incorporate several degrees of approximations in the solution of the HF equations. In this way, a very efficient algorithm has been constructed using the nearly HF multi-ζ exponential Clementi and Roetti's basis sets.[19] (b) With a localized solution it is easy and fruitful to partition the total energy of the system into atomic (ionic) and interatomic (interionic) contributions. This partition is used to obtain the crystal-adapted pair potentials employed in this work.[14] (c) As in weakly overlapping solids the correlation energy correction is almost entirely intra-atomic in nature (being therefore a sum of contributions from every group), then localized wave functions may be used to compute good size consistent estimates of this correction. In the present work, the correlation energy correction is obtained through Clementi's Coulomb-Hartree-Fock method,[20] as in all our previous computations of the EOS in pure crystals (MgO, ZnS, ZnO, alkali halides, etc).[13]

TABLE II. Short-range interatomic potentials employed in this work. Symbols correspond to the expression $\sum_k A_k e^{-\alpha_k r}$. Atomic units are used.

Pair	k	A_k	α_k
Ca^{2+}-F^-	1	200892.33	2.3865032
	2	-201695.22	2.3882894
F^--F^-	1	365.53615	0.86209675
	2	-364.81181	0.86168496

All simulations reported here describe the crystal at different fixed pressures in the static approximation (zero-temperature, zero-point contributions neglected). The appropriate thermodynamic potential to be used in these conditions is the Gibbs energy ($G_{T=0} = U + pV$), U being the internal energy (which in our approach is identified with the lattice energy, E_{latt}) and V the volume. The stable thermodynamic phase at a given T, p pair is that making the G function an absolute minimum with respect to all the geometrical parameters left free in the simulation. Moreover, any metastable phase must be a local minimum of the G potential in the multidimensional space defined by these parameters. Our computations range from $p = 0$ to $p = 15$ GPa in the C1 phase and from $p = 0$ to $p = 45$ GPa in the C23 phase, the ranges with available experimental data. When the volume and the internal energy are multivariable functions, it is not straightforward to obtain p through the relation $[p_{T=0} = -(dU/dV)_T]$, as is assumed in many solid-state calculations. In these cases, the EOS of a given system may be obtained from the G function. Taking the G energy as a function of every geometrical free parameter:

$$G = U(\mathbf{x}) + pV(\mathbf{x}), \tag{1}$$

where $\mathbf{x}$ is a vector with a whole set of geometrical parameters, and using p as a fixed constant, we can obtain the actual values of the $\mathbf{x}$ variables at the chosen p by minimizing the G function. Once we know the n-tuple p-$\mathbf{x}$ we get the volume through the $V(\mathbf{x})$ relation.

B. Geometry optimizations

To optimize the geometry, two different multidimensional minimization techniques have been used both at the pairwise and *ab initio* levels: downhill simplex and

modified Powell methods.[16] The former is a linearly convergent procedure based upon the construction of an initial $(N+1)$-dimensional $[(N+1)\mathrm{D}]$ convex polyhedron in the $(N+1)$D energy-geometrical parameter space, and its subsequent amoebic movement around the surface until the minimum is found. The latter is a renowned quadratically convergent scheme that iteratively minimizes the function of interest along 1D conjugate, noninterfering directions. It contains approximate formulas to estimate the gradient and Hessian of the hypersurface based on the function values found at the points explored.

The optimizations performed in the present work have been accomplished in two different manners. The time bottleneck in the *ab initio* computations is not associated with the internal work done by the optimizer, but with the calculation of each energy point requested. It is then very efficient to isolate the *ab initio* code from the optimizer and interconnect them through external calls to the operating system. This has led to the construction of a general, flexible minimization tool, OPTIM, able to optimize any multidimensional function computed by another external program without the need of modifying the external code. In pair-potential simulations the situation is reversed. In this case, the time consumed by the optimizer is comparable to that needed for the calculation of every energy point. The PAIRPOT code does therefore include the optimization procedures.

Our experience indicates that a good approach to internal energy or Gibbs energy optimizations in perfect crystals is a combined strategy mixing Powell and downhill simplex runs. When optimizing lattice parameters, the quadratically convergent Powell method usually gives the best time-quality ratio. However, the simplex scheme is better suited for the optimization of internal positions in the unit cell. This is due to the extensive geometric rearrangement of the atomic positions of a crystal induced by slight variations in the internal parameters. The energetic valleys associated with internal variables are deep and narrow. The shrinkage of a simplex in these situations allows passage through needle holes, while the Powell procedure does not.

All our optimizations start from zero-pressure conditions and continue by increasing the pressure up to the top limit noted above for the two phases. This allows the use of the optimum parameters found at a particular pressure value as starting points for the next minimization. For the $C1$ phase, since a single geometrical variable is involved, we have used the Powell scheme in *ab initio* as well as in pairwise calculations. The nine parameters of the $C23$ phase, however, represent a difficult task for a nonlinear optimization. We have started the simulation with PAIRPOT calculations, since this is an efficient procedure, on the scale of a tenth of a second per energy point (CPU times referred to a Convex C-120 vectorial machine) while the AIPI code runs in the scale of some minutes per point. The pairwise simulations help us as a guide for the otherwise blind attempts to reach minimum energy configurations in the quantum-mechanical hypersurface.

The exploration of the complicated 9D hypersurface of the $C23$ structure has forced us to devise two different optimization strategies. First, we began doing brute force 9D minimizations including random starting points and intuitive values based on parameters like those reported for the $PbCl_2$ crystal. Analysis of the results along this line have suggested a much cheaper scheme that has been proved to reach the same solutions, and which has been used as the standard strategy throughout this work. In this second procedure, we split the nine parameters into two exclusive sets: $S1$, formed of the cell parameters (a,b,c); and $S2$, formed of the internal coordinates $[x(\mathrm{Ca}),\ y(\mathrm{Ca}),\ x(\mathrm{F1}),\ y(\mathrm{F1}),\ x(\mathrm{F2}),\ y(\mathrm{F2})]$. In the G optimization process, the U or E_{latt} terms are $S1$ and $S2$ dependent, while the V term is only $S1$ dependent. Using the Powell method, we optimize the $S1$ variables while keeping frozen the $S2$ set to, for example, the experimental values of the $PbCl_2$ crystal. The $S1$ variables are then fixed and the $S2$ ones optimized using the simplex method, and the whole cycle is repeated until convergence in the two sets of parameters is reached. Experience shows that convergence is achieved in few cycles. The reason for this scheme to be so efficient is that the complexity of the 9D nonlinear optimization scales faster than linearly with the dimensions of the parametrical space.

C. Elastic constants

The computation of accurate values of the elastic constants of a crystal by means of numerical procedures is a complex task in general terms, due to the need for evaluation of second derivatives. Moreover, it is not easy to automate, since the expressions that need to be evaluated are very dependent on crystal symmetry. One way to overcome these difficulties is to obtain the Hessian matrix of the internal or Gibbs energy with respect to the lattice parameters $a, b, c, \alpha, \beta, \gamma$ in the usual crystallographic cell and then transform it to the elastic or effective elastic constant matrix, respectively.

An outline of this procedure follows. We define the elastic and effective elastic constants as

$$C_{ij} = \frac{\partial^2 U}{\partial \epsilon_i \partial \epsilon_j}, \tag{2}$$

$$C_{ij}^{\mathrm{eff}} = \frac{\partial^2 G}{\partial \epsilon_i \partial \epsilon_j}, \tag{3}$$

where ϵ_i refers to the Voigt components of the Lagrangian strain parameters:[21]

$$\epsilon_1 = \epsilon_{11},\ \epsilon_2 = \epsilon_{22},\ \epsilon_3 = \epsilon_{33},$$
$$\epsilon_4 = 2\epsilon_{23},\ \epsilon_5 = 2\epsilon_{13},\ \epsilon_6 = 2\epsilon_{12}. \tag{4}$$

Dimensionless lattice parameters $\{\eta_i\}$ may be introduced:

$$\eta_1 = a/a_0,\ \eta_2 = b/b_0,\ \eta_3 = c/c_0,$$
$$\eta_4 = \alpha,\ \eta_5 = \beta,\ \eta_6 = \gamma, \tag{5}$$

with (a_0, b_0, c_0) the lattice constants of the solid at a given fixed point chosen as the origin of the elastic deformation. The elastic constants in the cell's reference frame are then obtained from the U or G Hessian matrices through the following expression:

$$C_{ij} = \frac{1}{V}\left\{\sum_{kl}\frac{\partial^2 U}{\partial\eta_k\partial\eta_l}\frac{\partial\eta_k}{\partial\epsilon_i}\frac{\partial\eta_l}{\partial\epsilon_j} + \sum_{k}\frac{\partial U}{\partial\eta_k}\frac{\partial^2\eta_k}{\partial\epsilon_i\partial\epsilon_j}\right\}, \quad (6)$$

where the matrices relating the η's to the ϵ's can be easily obtained from the definition of the Lagrangian parameters.[21] It should be noted that in the analog to Eq. (6) for C_{ij}^{eff}, the second term on the right-hand side vanishes.

The transformation of the elastic constants computed in the crystallographic frame to the usual orthogonal reference frame can be done now in a straightforward manner taking into account the contravariant properties of the C_{ij} under coordinate changes. For example, the elastic constants of the $C1$ phase in the orthogonal cell (F) are obtained from those in the primitive cell (P) by means of the following expression:

$$C_{ijkl}^{F} = \sum_{mnop} C_{mnop}^{P} M_{im} M_{jn} M_{ko} M_{lp}, \quad (7)$$

where we have not used Voigt contracted coefficients, and where M is the matrix relating the primitive cell unit vectors to the face centered ones:

$$M = \frac{1}{\sqrt{2}}\begin{pmatrix} 1 & 0 & 1 \\ 1 & 1 & 0 \\ 0 & 1 & 1 \end{pmatrix}. \quad (8)$$

To compute the derivatives, we have used a Richardson extrapolation algorithm. With the same spirit already described, a derivatives code (DERIVE) (Ref. 15) has been constructed as an external general tool, able to obtain first- and second-order derivatives of any function computed by another program. We have obtained in this way the C_{11} and C_{12} effective elastic constants of the $C1$ phase. C_{44} involves an inner strain and implies the expensive optimization of atomic positions inside the cell at each point requested in the derivation process. Since C_{44} does not enter in the bulk modulus expression, $B = (C_{11}^{\text{eff}} + 2C_{12}^{\text{eff}})/3$, our main concern about elastic constants in this work, it will not be considered here.

III. RESULTS AND DISCUSSION

A. The cubic phase

1. Zero T and p cohesive and elastic properties

For the $C1$ fluorite-type structure of CaF_2 there is a number of zero-pressure observable properties which can be immediately calculated with the computational tools described above. Results are gathered in Table III, where we include room temperature observed values,[7,22–25] and extrapolations to 0 K of experimental data,[23–27] since these are the appropriate values to compare with our static predictions. We have also introduced a column with the results obtained by Catti *et al.*[28] from *ab initio* periodic HF-type calculations, as implemented in the CRYSTAL program.[29] The room temperature data for the

TABLE III. Equilibrium properties of CaF_2 at zero pressure for the $C1$ phase.

	Calculated			Experimental	
	PAIRPOT	AIPI	CRYSTAL[a]	0 K	Room T
a (Å)	5.563	5.444	5.538	5.444[b]	5.463[c]
E_{latt} (kJ/mol)	2611.2	2638.7	2590	2622[d]	2585[e]
C_{11} (GPa)	150.4	171.4	172.2	173.0[f]	165.5[g]
				174.8[h]	165.1[i]
				172[j]	164.2[j]
C_{12} (GPa)	51.8	38.3	38.6	40.5[f]	38.9[g]
				47.9[h]	44.5[i]
				46.6[j]	43.98[j]
B_0 (GPa)	84.7	82.7	82.6	84.7[f]	81.1[g]
				90.2[h]	84.7[i]
				88.7[j]	84.1[j]
B_0'	4.2	4.0			4.92[j]

[a]Reference 28.
[b]Reference 26.
[c]Reference 7.
[d]Reference 27.
[e]Reference 22.
[f]0 K extrapolation by Catti *et al.* (Ref. 28) from higher T data of Ref. 23.
[g]Reference 23.
[h]0 K extrapolation by Catti *et al.* (Ref. 28) from higher T data of Ref. 24.
[i]Reference 24.
[j]Reference 25. These authors obtained the 0 K experimental values using their data at 298 K and 195 K.

elastic constants, bulk modulus, and its first derivative are adiabatic values obtained from Brillouin scattering[23] and ultrasonic experiments.[24,25] The 0 K extrapolated values for these properties have been calculated by Catti *et al.*[28] from the higher T adiabatic data of Refs. 23, 24, and by Wong and Schuele using their adiabatic measurements at 195 K and 298 K.[25] We have verified that the 0 K extrapolations of the higher T isothermal values given by Ho and Ruoff[24] coincide with the adiabatic extrapolations within 1 GPa.

From Table III it is observed that the three experimental C_{11} values are rather similar. However, for C_{12} there exists discrepancy between the 0 K extrapolation from Catlow *et al.* experiments[23] (40.5 GPa) and those from the ultrasonic data[24,25] (47.9 GPa, 46.6 GPa). This discrepancy is transferred by means of the $B_0 = (C_{11} + 2C_{12})/3$ formula to the bulk modulus, although the relative differences between the three extrapolated values for this property are smaller than for C_{12}: 84.7 (Ref. 23), 90.2 GPa (Ref. 24), and 88.7 GPa (Ref. 25). The isothermal bulk modulus is also accessible from the fitting of empirical equations to p-V data. Thus, the Murnaghan EOS derived from the room temperature measurements of Angel[8] produces a value of 81±1.2 for B_0, which agrees with the room temperature isothermal value of 81.7 GPa obtained from the ultrasonic measurements of Wong and Schuele.[25] Therefore, Angel's results would suggest that the athermal value for B_0 was closer to 90 GPa, as in the ultrasonic experiments, than to 85 GPa, as in the Brillouin scattering measurements. We believe, however, that both extrapolated values are not sufficiently different from each other to refuse one in favor of the other.

The set of theoretical predictions shows a quite satisfactory agreement with the corresponding 0 K extrapolations from experimental data at higher T. AIPI and CRYSTAL results do not differ appreciably from each other, although the AIPI computed equilibrium lattice parameter and lattice energy are closer to the experiments. The same behavior was already found in the calculation of the EOS on the ZnS rocksalt ($B1$) structure.[30] Our AIPI predictions (38.3 for C_{12} and 82.7 for B_0), as well as those of Catti *et al.*[28] (38.6 GPa and 82.6 GPa), are closer to the data of Catlow *et al.*[23] than to the values from ultrasonic experiments.[24,25] The predictions using interatomic potentials (PAIRPOT from now on) present some discrepancies for the elastic constants, but the overall comparison, including the bulk modulus, is again very reasonable.

Catti *et al.*[28] argue that their somewhat high value for a is probably related to the neglect of electron correlation and atomic polarization effects in the CRYSTAL calculation. In fact, the inclusion of correlation energy corrections improves the prediction of the equilibrium lattice parameter, as Aprà *et al.*[31] have recently illustrated in their analysis of the correlation effects in CRYSTAL computations on the NaCl EOS. They concluded that consideration of correlation moves inwards at least 4.6% the computed equilibrium lattice parameter of the $B1$ structure of NaCl. However, it is not only on the equilibrium geometry where the correlation effects modify their HF predictions. On NaCl, differences as great as 30% are obtained for the bulk modulus between CRYSTAL calculations at the HF and the HF+correlation correction level.[31] Therefore, the inclusion of correlation effects in the CRYSTAL calculations of the $C1$ phase of CaF_2 could bring a into better agreement with the experiment value, but, at the same time, it could significantly reduce the quality of the predictions for the elastic constants and the bulk modulus. In the computations performed with the AIPI method, the equilibrium lattice parameter, and the isothermal bulk modulus change from 5.61 Å and 66 GPa to 5.44 Å and 82.7 GPa, respectively, when the correlation energy corrections are taken into account. It is to be noticed that in our case both magnitudes show simultaneously a better agreement with the experimental data after the corrections of the correlation energy are included.

2. *Pressure dependence of the elastic constants for the C1 phase*

The behavior of the effective elastic constants (C_{11}^{eff} and C_{12}^{eff}) and the bulk modulus (B) at different pressures has also been explored for the $C1$ phase of CaF_2 up to 10 GPa. According to our calculations, C_{ij}^{eff}-p and B-p curves are increasing functions that can be very accurately represented as second-order polynomial in pressure. Our calculations provide positive first derivatives and negative second derivatives for the C_{ij}^{eff}-p and B-p curves. The first derivatives from AIPI computations are 4.6, 3.8, and 4.0, and the second derivatives -0.086 GPa^{-1}, -0.050 GPa^{-1}, and -0.053 GPa^{-1} for C_{11}, C_{12} and B, respectively. Thus, we obtain a small contribution of the p^2 term for the elastic constants and the bulk modulus. We want to stress that the pressure dependence of the bulk modulus has been calculated by two different methods that have provided the same set of values within 0.15 GPa: (i) using the second derivative of the Gibbs energy with respect to the volume, and (ii) using the elastic constant relation given above.

To the best of our knowledge, the available experimental data[24,25] are restricted up to 0.4 GPa. Ho and Ruoff pointed out that, at least for the second derivatives, their data should not be taken quantitatively.[24] Wong and Schuele[25] reported the first pressure derivative for the bulk modulus at 195 K (4.76) and 298 K (4.92) which suggests a positive B_0'-T slope and a 0 K value for this magnitude of 4.5. The room T value is similar to that found by Angel for the isothermal B_0' (5.22±0.35).[8] Values for B_0' given by Ho and Ruoff[24] decrease from 6.08±0.27 at 295.5 K to 4.60±0.06 at 194.5 K, but at 77.35 K B_0' increases up to 5.48±0.16. An extrapolation using their data at 295.5 K and 194.5 K gives a value of 1.8 for this magnitude at 0 K. Our computed values [4.2 (PAIRPOT) and 4.0 (AIPI)] are consistent with the expected extrapolation to the athermal limit from the data of Wong and Schuele.[25] Finally, Dutt, Kaur, and Shanker[32] have evaluated the first and second pressure derivatives of B_0 using a collection of available interatomic potentials for CaF_2. Their values of 4.0±0.7 for B_0' and -0.060±0.006 for B_0'' are very similar to the corresponding values from AIPI computations.

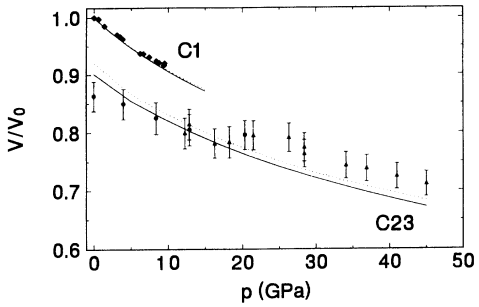

FIG. 1. Static V/V_0-p diagrams for $C1$ and $C23$ phases of CaF_2 according to PAIRPOT (dotted) and AIPI (solid) calculations, and experimental values (symbols) from Ref. 9. Triangles and circles stand for data at increasing and decreasing pressure, respectively.

TABLE IV. Equilibrium properties of CaF_2 at zero pressure for the $C23$ phase. Experimental values at room temperature from Ref. 9.

	PAIRPOT	AIPI	Experimental
a (Å)	7.109	7.014	7.15±0.07
b (Å)	6.069	5.860	5.63±0.11
c (Å)	3.643	3.540	3.49±0.03
x (Ca)	0.113	0.116	
y (Ca)	0.246	0.249	
x (F1)	0.425	0.428	
y (F1)	0.354	0.356	
x (F2)	0.667	0.673	
y (F2)	0.979	0.973	
E_{latt} (kJ/mol)	2595.7	2630.1	
B_0 (GPa)	86	86	
B_0'	4.1	4.1	

3. Equation of state for the C1 phase

Concerning the EOS, we have adopted the usual V/V_0-p curve to represent the crystal response to pressure, V_0 being the zero-pressure volume of the $C1$ structure (see Fig. 1). A number of other plots may be carried out[13] including the $V(T)/V_0(T)$ versus $p/B_0(T)$ diagram, which was found to be quite useful to represent in the same scale static 0 K and room temperature data for the alkali chlorides. For the cubic polymorph of CaF_2 the observed values of B_0 show a small T dependence, as discussed above. We have verified that the $V(T)/V_0(T)$ versus p/B_0 diagram compares with the experimental data in the same way as the V/V_0 versus p curve does. Therefore, we have adopted the V/V_0 versus p diagram in order to include in the same plot the information about the $C23$ phase, where the B_0 experimental value is not available.

In this normalized volume diagram, both AIPI and PAIRPOT curves agree with the recent room T single-crystal and powder x-ray data reported by Gerward *et al.*[9] The p-V measurements by Angel[8] do not differ from the data of Gerward *et al.* When we use absolute volumes, the quantitative agreement with the experiments is not so good for the PAIRPOT computations due to the worse prediction of the zero-pressure lattice parameter in this type of calculation. However, once the disagreement of V_0 is absorbed into the V/V_0 ratio, the PAIRPOT curve matches the experimental EOS since B_0 is predicted accurately.

B. The orthorhombic phase

1. Zero T and p cohesive properties

As we did with the $C1$ phase, we first collect for the $C23$ phase (Table IV) zero-pressure information from our static computations (PAIRPOT and AIPI) and experimental measurements. This structure has been retained as a metastable phase at ambient conditions, after releasing pressure, in the high-pressure experiments performed by Gerward *et al.*[9] They have measured the unit cell lengths (a, b, c) with larger uncertainties than for the cubic phase due to the fact that the x-ray spectra were carried out on crystalline powder in the $C23$ phase. The internal coordinates for Ca, F1, and F2 have not been reported yet. Besides, the uncertainties in the molar volume preclude a reliable determination of the bulk modulus and its first pressure derivative through empirical EOS fitting.

Our computed values in Table IV constitute, therefore, the first full structural characterization of the orthorhombic phase of CaF_2. The difference between PAIRPOT and AIPI predictions for (a, b, c) is very similar to that found for the lattice parameter a in the $C1$ phase. The comparison with the experimental data is very satisfactory, with discrepancies less than 4% in the case of the AIPI results. For the zero-pressure bulk modulus and its first derivative, we have obtained the same values, 86 GPa and 4.1, respectively, in the PAIRPOT and AIPI approaches. The prediction for B_0 is only 2–3 GPa greater than the value found for the $C1$ phase. This result gives rise to a small change of B along the $C1$-$C23$ phase transition, as we will document below.

2. Equation of state for the C23 phase

In the V/V_0-p diagram of Fig. 1, we plotted the experimental and computed response to pressure of the $C23$ phase of CaF_2. The error bars in the experimental data are obtained using the mean error ($\Delta l/l = 10^{-2}$) associated with the measurements of the unit cell lengths (l). In the curves for the $C23$ phase, V_0 is the corresponding zero-pressure volume of the $C1$ phase in the experimental, PAIRPOT, and AIPI determinations.

As noted before, PAIRPOT and AIPI curves show very similar slopes in the studied range (0–45 GPa): they are parallel to each other and parallel to the corresponding $C1$ curves. The $C23$ observed data do not follow such a trend, although the large uncertainties in the $C23$ volume do not exclude the parallel behavior to be physically true. The mean observed values suggest a less compressible solid (higher bulk modulus) in the $C23$ phase. Nevertheless, we note that, except for the zero-pressure point, the experimental information up to 20 GPa strad-

dles the two theoretical computed curves. Above 20 GPa, the PAIRPOT and AIPI predictions lie slightly below the experimental error bars. It is interesting to point out that an overestimation of the density of the high-pressure phase was also found by Bukowinski[33] as the most common result of theoretical EOS for compounds having pressure-induced $B1$-$B2$ phase transitions. For the alkali chlorides, we have shown that the differences between observed and computed values at high pressures were mainly due to thermal effects.[13] This may be also the case here. Unfortunately, we are unable to perform the same analysis since B_0 for the $C23$ phase has not been experimentally determined at room temperature.

Further experiment-theory comparisons are provided by plotting the specific values of the three unit cell lengths (a, b, c) versus p (see Fig. 2). First of all, we observe again that the general view is very satisfactory. Most of the experimental data lie between the AIPI and PAIRPOT curves. These curves help to understand more clearly the global behavior of (a, b, c), since from the experimental data it is not possible to conclude that the three lattice parameters decrease continuously as pressure is applied. According to the AIPI calculations, the reduction of a, b, and c is of 8.4%, 9.0%, and 9.3%, respectively, in the range 0–45 GPa.

It is also interesting to remark that our careful optimization strategies have provided a qualitatively consistent picture, with optimized configurations showing soft dependence on pressure. This is not the general case, even for static simulations, when dealing with *ab initio* techniques and multivariable surfaces. If, for example, the zero-pressure set of optimized parameters is used as the starting choice for the optimizations in the whole range of pressures, the curves would keep the same trends but would also present sharp discontinuities.

The results obtained for the internal coordinates in the range 0–45 GPa show that the six variables change slightly with pressure. This is the expected behavior on the basis of the smaller influence of these parameters on the Gibbs potential, as we pointed out in Sec. II. The AIPI computations in the range of 0–45 GPa give variations not bigger than 3% for the set of the internal coordinates, with specific values at 45 GPa of 0.119 [x(Ca)], 0.251 [y(Ca)], 0.430 [x(F1)], 0.350 [y(F1)], 0.676 [x(F2)], and 0.960 (y(F2)). The comparison with the 0 GPa values collected in Table IV shows that only the y components of the fluorine ions decrease with pressure.

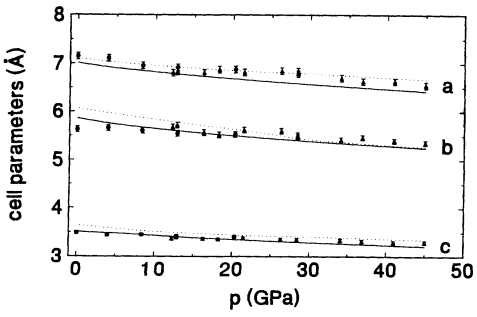

FIG. 2. Pressure dependence of the three unit cell lengths of the $C23$ phase of CaF_2 according to PAIRPOT (dotted) and AIPI (solid) calculations, and experimental values (symbols) from Ref. 9. Triangles and circles stand for data at increasing and decreasing pressure, respectively.

3. *Simulation of the x-ray diffraction spectrum for the C23 phase*

Although no experimental data are available for the internal coordinates of the $C23$ phase of CaF_2, Gerward *et al.*[9] have reported the diffraction intensities assigned to some of the peaks observed in their x-ray experiments on CaF_2 powder at 45 GPa. Bearing in mind the difficulties due to poor grain statistics, problems of preferred orientation, and those inherent to the energy-dispersive technique, it may be interesting to tentatively associate those intensities with the computed positions of the atoms in the unit cell.

In order to perform such a comparison, we have calculated a theoretical x-ray diffraction spectrum using the AIPI optimized set of nine parameters at 45 GPa. This simulation, carried out with the program LAZY-PULVERIX,[34] is illustrated in Fig. 3. We have explored the role of some external parameters, such as temperature, scattering, and geometrical correction factors, with the aim of adapting our simulation to the actual experiment conditions described in Ref. 9. Thus, we have taken from Hazen and Finger[7] the isotropic temperature factors of Ca^{2+} (B_{Ca}=0.54 Å^2) and F^- (B_F=0.76 Å^2) obtained for the CaF_2 $Fm3m$ structure at 296 K. The choice of these parameters was checked against the absence of temperature factors concluding that their influence is negligible. The scattering factors were derived from the AIPI electronic densities of Ca^{2+} and F^- in the $Pbnm$ structure at 45 GPa. The use of the standard tabulated scattering factors, based on free ion electronic densities,[35] changed the absolute values of the computed intensities, but the general aspect of Fig. 3 was not modified. Finally, the intensities (I) were corrected using the appropriate expression according to the energy-dispersive method used by Gerward *et al.*:[9]

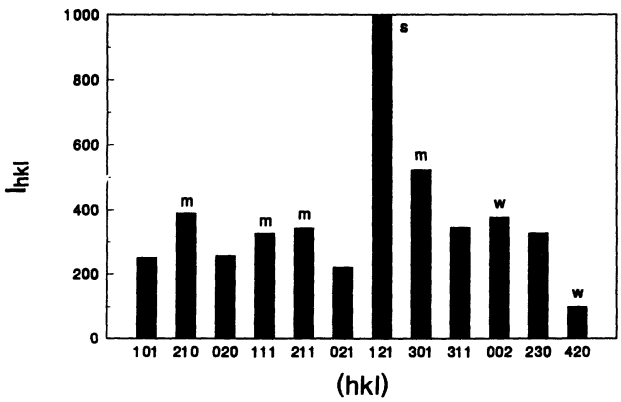

FIG. 3. AIPI simulation of the x-ray diffraction spectra for the $C23$ phase of CaF_2 at 45 GPa. The s (strong), m (medium), and w (weak) labels denote the intensities reported by Gerward *et al.* in Ref. 9.

$$I_{hkl}(\text{corr}) = I_{hkl} \times d_{hkl}^2, \quad (9)$$

where d_{hkl} is the distance between planes (hkl).

We find a good correlation between the observed intensities [denoted by s (strong), m (medium), and w (weak)] and the predictions from the simulated x-ray spectrum (see Fig. 3). Only one of the lines assigned as weak in the experiments should be included in the set of lines with medium intensities according to our computed spectrum. In addition, we have found some other lines of intensities in the weak-medium interval not reported by Gerward *et al.* The reason to explain that absence might be the weakness of those lines and (or) the reduction of line detections in anvil-cell experiments.[7] Our global conclusion from this computer experiment, along with the previous analysis of the $C23$ phase data, is that the computed lattice parameters (a, b, c) and the internal coordinates are consistent with the reported experimental information. These numerical values constitute a theoretical characterization of the *Pbnm* structure of CaF_2 that warrants further experimental efforts.

C. Stability and transition phase data

There are several experimental evidences confirming the pressure-induced first-order phase transition displayed by CaF_2 from the cubic $Fm3m$ structure to the orthorhombic *Pbnm* one. The two most recent high-pressure measurements reported $C1$-$C23$ transition pressures in the range from 7.75 GPa (Ref. 8) to 9.5 GPa (Ref. 9). This phase transformation was previously detected between 8 and 10 GPa by Seifter[36] and Dandekar and Jamieson.[37] The last authors were not able to see lines from the *Pbnm* structure in diffraction patterns taken at one bar on previously pressurized samples. Angel[8] has also described the *Pbnm* phase response to pressure release, indicating that the $C23$ phase reverted to the $C1$ phase. However, it is clear from the experiments of Gerward *et al.*[9] that the high-pressure phase can be retained at ambient conditions, although they pointed out that the reversibility varies greatly from experiment to experiment. The quenchability of this transformation must be linked to the presence of thermal activation barriers in the transition path connecting $C1$ and $C23$ phases.

Unfortunately, the great number of degrees of freedom present in the orthorhombic structure precludes a reliable microscopic exploration of the transition mechanism, as we have recently performed for the $B1$-$B2$ transition in the alkali halide crystals.[38] However, valuable qualitative information is general for this kind of structural first-order transitions. We observe, for example, that the transformation is accompanied by an increase of the coordination numbers of the cation, which is quasi-nine-coordinated in the *Pbnm* structure (eight in the $Fm3m$), and one of the fluorines, which is five- and four-coordinated in the *Pbnm* and in the $Fm3m$ structures, respectively. The mean Ca-F nearest-neighbor distance at 0 GPa increases from $C1$ to $C23$ but the molar volume decreases around 10%. These facts respond to the behavior observed in the $B1$ and $B2$ phases of the alkali halide crystals.

The rearrangement in the environment of each ion in the lattice yields to the breaking and creation of bonds and can be considered as the *inertia* (activation energy) of the crystal to maintain its current structure. As discussed in our study of the $B1$-$B2$ transition path,[38] to overcome the activation barrier we have to supply the corresponding thermal energy to the crystal. For a given temperature, we can observe the $C1$-$C23$ transition by increasing pressure, as the magnitude of the barrier decreases in that direction. This general overview of the real transition is necessary in order to understand which is the information that static thermodynamic analysis can provide.

Regarding equilibrium and static conditions, the thermodynamic transition pressure is reached when the Gibbs energies of both phases are the same. This situation is achieved before the $C1 \rightarrow C23$ and after the $C23 \rightarrow C1$ transitions are observed at the laboratory conditions. Therefore, the computed thermodynamic transition pressure must lie between the observed values of the direct and reverse transition, i.e., in the range from 0–10 GPa. Furthermore, this range should become narrower as the temperature increases, since the available thermal energy of the crystal also increases with T.

Our results are depicted in Fig. 4. The G-p curves show that the $C1$ phase is the most stable up to 4 GPa (AIPI) and 7 GPa (PAIRPOT). The stabilization energy (the difference between the $C1$ and $C23$ Gibbs energy) is as small as 7.6 kJ/mol (AIPI) and 15.5 kJ/mol (PAIRPOT) at 0 GPa, and shows a slight dependence on pressure. This is the behavior found in the $B1$-$B2$ phase transition of alkali halides.[13] The volume reduction at the transition pressure is about 10% in both types of calculations. This number compares well with the observed values of Gerward *et al.*[9] (11%) and Dandekar and Jamieson[37] (10%). The absolute values of the bulk modulus at the AIPI transition point are 98.4 GPa ($C1$) and 102.4 GPa ($C23$), yielding an increase of this magnitude of about 4% which has no experimental counterpart.

We see that the theoretical predictions are consistent with the previous description of the first-order structural phase transitions. Our computations provide a safe start-

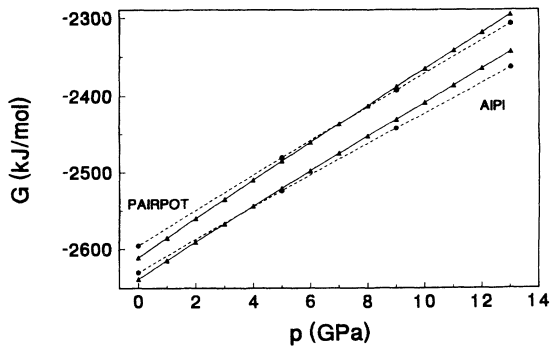

FIG. 4. Phase stability of CaF_2 according to PAIRPOT and AIPI calculations. Triangles and circles stand for discrete values of the $C1$ (solid) and $C23$ (dashed) phases, respectively.

ing point that may be used in both static and dynamics simulations directed to the exploration of the mechanism of this transformation.

IV. CONCLUSIONS AND PROSPECTS

We have addressed the global description of the 0 K EOS of CaF_2 using two different first-principles approaches to the total energy of a perfect crystal. In the PAIRPOT calculations, we have employed crystal adapted interatomic potentials developed from a nonempirical procedure.[14] In the AIPI scheme,[11,17] the Hartree-Fock equations of the solid are solved in a localized (ionic) Fock space and the correction of the correlation energy is estimated by means of the Coulomb-Hartree-Fock method.[20] Both theoretical procedures have been efficiently combined with numerical tools able to seek the extrema of the $(N+1)$D energy-geometrical parameters surfaces and to perform accurately the appropriate derivatives for the Hessian of the Gibbs matrix.

The 0 K static EOS of the cubic fluorite-type and the orthorhombic α-$PbCl_2$-type polymorphs observed in CaF_2 have been determined with the PAIRPOT and AIPI procedures in the range where the experimental information is available. The elastic behavior and its pressure dependence has also been explored for the cubic structure.

Our set of interatomic potentials has successfully predicted a collection of cohesive and elastic properties, and has provided a consistent description of the p-V and the phase transition data. The PAIRPOT calculations have been in our study a firsthand tool preceding AIPI computations, mainly in the search of reliable solutions within the 9D surface of the α-$PbCl_2$-type polymorph.

Concerning the AIPI approach, the results obtained for the cohesive and structural magnitudes in the two polymorphs of CaF_2 maintain the uniformly good quality shown in the variety of compounds where this model has been previously used. Interesting conclusions from our results were drawn specifically in the following three areas: (a) The EOS of the $C1$ and $C23$ phases. The quantitative agreement of our computed EOS with the observed data evidences the reliability of the combined strategy proposed in this investigation: PAIRPOT-AIPI for total energy calculations plus downhill simplex and modified Powell methods for the multidimensional optimizations. (b) The full characterization of the crystal parameters for the α-$PbCl_2$-type polymorph. The three unit cell lengths and the six internal coordinates of this structure have been given here for the first time and have provided a simulated x-ray diffraction spectrum which is consistent with the available information for this phase. (c) The pressure-induced transition phase. Our computations reveal a parallelism between the $C1$-$C23$ transformation and the $B1$-$B2$ transition explored in the alkali chlorides:[13,38] the stable phase at 0 GPa is correctly predicted, the thermodynamic transition pressure lies within the range of pressures for the direct and reverse transitions, the volume reduction at the transition point is about 10%, etc. These facts are again in agreement with the observed behavior.

For the work to come, there are natural options both in the superionicity and pressure calibration subjects that are still open. The static simulation presented here should be complemented with a molecular dynamics study directed at the description of the phenomena involved in the ionic conductivity as T increases. The project is, of course, not new, but it has not been undertaken with explicit consideration of the pressure as a variable of the system. The loss of the superionic state along the $C1$-$C23$ transition in the CaF_2 crystal may be considered as a next step to investigate using our interionic potentials in molecular dynamics calculations.

The most interesting challenge concerning the structural and mechanical properties of these two polymorphs is the general understanding of the phase transition mechanism, in the manner we have undertaken for the $B1$-$B2$ transformation of the alkali halides.[38] Although the problem is here much more complex (and less known), the analysis of the changes in simulated x-ray diffraction spectra, analogous to the one of Fig. 3, and/or the use of molecular dynamics simulations can guide us to trace back the transition path. Finally, using the computational tools we have presented in this work, the question of the relative stability of both polymorphs may be addressed by means of the Gibbs Hessian matrix or by analyzing the effect of pressure on the effective elastic constants, in particular the C_{44} (inner strain dependent) response to pressure.

ACKNOWLEDGMENTS

We are especially grateful to Professor L. Gerward for comments and sending us detailed numerical data of the investigation reported in Ref. 9. Thanks are due to M. A. Salvadó who assisted us in the computational simulation of the x-ray diffraction spectra. All calculations have been done on the Convex C-120 (Centro del Cálculo Científico) and HP9000 (Centro de Cálculo) computer facilities at the Universidad de Oviedo. Financial support from the Spanish Dirección General de Investigación Científica y Técnica (DGICYT), Project No. PB90-0795, is also acknowledged.

[1] J. Oberschmidt and D. Lazarus, Phys. Rev. B **21**, 2952 (1980); **21**, 5813 (1980); **21**, 5823 (1980).
[2] M. T. Hutchings, K. Clausen, M. H. Dickens, W. Hayes, J. K. Kjens, P. G. Schnabel, and C. Smith, J. Phys. C **17**, 3903 (1984).
[3] Y. Bouteiller, Phys. Rev. B **45**, 8734 (1992).
[4] F. Shimojo and H. Okazaki, J. Phys. Condens. Matter **5**, 3405 (1993).
[5] M. Parrinello, A. Rahman, and P. Vashishta, Phys. Rev. Lett. **50**, 1073 (1983).

[6] P. J. D. Lindan and M. J. Gillan, J. Phys. Condens. Matter **5**, 1019 (1993).
[7] R. M. Hazen and L. W. Finger, J. Appl. Cryst. **14**, 234 (1981).
[8] R. J. Angel, J. Phys. Condens. Matter **5**, L141 (1993).
[9] L. Gerward, J. S. Olsen, S. Steenstrup, M. Malinowski, S. Asbrink, and A. Waskowska, J. Appl. Cryst. **25**, 578 (1992).
[10] R. J. Angel, N. L. Ross, I. G. Wood, and P. A. Woods, Phase Trans. **39**, 13 (1992).
[11] V. Luaña and L. Pueyo, Phys. Rev. B **41**, 3800 (1990).
[12] V. Luaña, A. Martín Pendás, J. M. Recio, E. Francisco, and M. Bermejo Comput. Phys. Commun. **77**, 107 (1993).
[13] J. M. Recio, A. Martín Pendás, E. Francisco, M. Flórez, and V. Luaña, Phys. Rev. B **48**, 5891 (1993), and references therein.
[14] J. M. Recio, E. Francisco, M. Flórez, and A. Martín Pendás, J. Phys. Condens. Matter **5**, 4975 (1993).
[15] V. Luaña, M. Flórez, and L. Pueyo, J. Chem. Phys. **99**, 7970 (1993).
[16] W. H. Press, B. P. Flannery, S. A. Teukolsky, and W. T. Vetterling, *Numerical Recipes* (Cambridge University Press, New York, 1986).
[17] V. Luaña, M. Flórez, E. Francisco, A. Martín Pendás, J. M. Recio, M. Bermejo, and L. Pueyo, in *Cluster Models for Surface and Bulk Phenomena*, Vol. 283 of *NATO Advanced Study Institute, Series B: Physics*, edited by G. Pacchioni, P. S. Bagus, and F. Parmigiani (Plenum, New York, 1992), p. 605.
[18] C. Pisani, R. Dovesi, and C. Roetti, *Hartree-Fock ab initio Treatment of Crystalline Systems*, Vol. 48 of *Lecture Notes in Chemistry* (Springer-Verlag, Berlin, 1988).
[19] E. Clementi and C. Roetti, At. Data Nucl. Data Tables **14**, 177 (1974).
[20] S. J. Chakravorty and E. Clementi, Phys. Rev. A **39**, 2290 (1989), and references therein.
[21] D. C. Wallace, *Thermodynamics of Crystals* (John Wiley, New York, 1972).
[22] J. Shanker, J. P. Shing, and V. C. Jain, Physica (Utrecht) B **106**, 247 (1981).
[23] C. R. A. Catlow, J. D. Commins, F. A. Germano, R. T. Harley, and W. Hayes, J. Phys. C **11**, 3197 (1978).
[24] P. S. Ho and A. L. Ruoff, Phys. Rev. **161**, 864 (1967).
[25] C. Wong and D. E. Schuele, J. Phys. Chem. Solids **29**, 1309 (1968).
[26] G. K. White, J. Phys. C **13**, 4905 (1980).
[27] R. C. Weast, *Handbook of Chemistry and Physics*, 64th ed. (Chemical Rubber Co., Boca Raton, 1983).
[28] M. Catti, R. Dovesi, A. Pavese, and V. R. Saunders, J. Phys. Condens. Matter **3**, 4151 (1991).
[29] CRYSTAL 88, Quantum Chemistry Program Exchange (Indiana University, Bloomington, IN, 1989), Program No. 577.
[30] J. M. Recio, R. Pandey, and V. Luaña, Phys. Rev. B **47**, 3401 (1993).
[31] E. Aprà, M. Causà, M. Prencipe, R. Dovesi, and V. R. Saunders, J. Phys. Condens. Matter **5**, 2969 (1993).
[32] N. Dutt, A. J. Kaur, and J. Shanker, Phys. Status Solidi B **137**, 459 (1986).
[33] M. S. T. Bukowinski, Geophys. Res. Lett. **12**, 536 (1985).
[34] K. Yvon, W. Jeitschko, and E. Parthe, J. Appl. Cryst. **10**, 73 (1977).
[35] *International Tables for Crystallography*, edited by J. A. Ibers and W. C. Hamilton (Kluwer Academic Publishers, Dordrecht, 1989) Vol. IV.
[36] K. F. Seifert, Ber. Bunsenger, Physik Chem. **70**, 1041 (1966).
[37] D. P. Dandekar and J. C. Jamieson, Trans. Am. Crystallogr. Assoc. **5**, 19 (1969).
[38] A. Martín Pendás, V. Luaña, J. M. Recio, M. Flórez, E. Francisco, M. A. Blanco, and L. N. Kantorovich, Phys. Rev. B **49**, 3066 (1994).